Low-Voltage, High-Frequency Organic Transistors and Unipolar and Complementary Ring Oscillators on Paper

Ulrike Kraft,* Tarek Zaki, Florian Letzkus, Joachim N. Burghartz, Edwin Weber, Boris Murmann, and Hagen Klauk

Paper substrates for flexible, mobile, and disposable electronic applications draw academic and commercial attention due to their many advantages, such as cost efficiency, low weight, mechanical flexibility, and environmental compatibility. For portable electronic applications, it is important that the electronic devices and circuits can be operated with voltages of a few volts, due to the limitations of mobile power supplies, such as solar cells or energy harvesting devices. Here, low-voltage organic p-channel and n-channel transistors as well as unipolar and complementary ring oscillators are fabricated directly on the surface of a banknote. It is demonstrated that low-power organic integrated circuits on paper substrates can be operated with supply voltages of less than 3 V and with frequencies of several hundred kilohertz. These results emphasize the prospects of organic transistors for smart paper applications.

1. Introduction

Paper has been used by humans for more than 2000 years,[1] and over the centuries, various types of paper and a wide range of applications for paper have been developed. Paper has the advantages of being a lightweight, low-cost, robust, bendable, foldable, renewable, and biodegradable material. By implementing electronic functionality in the form of sensors, displays, or circuits on paper, flexible smart paper can be created. Possible applications that combine the sensing or display functionalities of electronics with the utility of paper[2] can be found in consumer packaging, food safety,[3,4] or medical sensing (e.g., glucose, lactate, and uric acid analysis[3,5]). Another potential application is the addition of active electronic

anti-counterfeiting or tracking features to the existing passive security features on banknotes.[6] One possibility for implementing active electronic circuits on paper is the use of organic thin-film transistors (TFTs), since these can usually be fabricated at relatively low temperatures, which simplifies their fabrication on temperature-sensitive substrates, such as paper.

Organic TFTs have been successfully fabricated on various types of paper, including commercial packaging paper,[2] printing paper,[7–9] photo paper,[10–14] homemade paper,[15,16] starch paper,[17] and banknotes.[6,18] In some cases, one or several coatings were applied to the surface of the paper prior to TFT fabrication in order to smoothen or seal the surface.[2,10–13,19,20] For example, Li et al. fabricated bottom-gate, top-contact TFTs based on solution-processed C_8-BTBT on parylene-coated photopaper and reported a carrier mobility of 1.3 cm^2 $(Vs)^{-1}$ and an on/off current ratio of 10^8.[13] Minari et al. used parylene-coated photopaper as the substrate and fabricated top-gate TFTs using drop-cast C_8-BTBT as the semiconductor and Au nanoparticles for the source and drain contacts and measured a carrier mobility of 2.5 cm^2 $(Vs)^{-1}$.[20] This is still the highest carrier mobility reported to date for organic transistors on paper. Grau et al. demonstrated roll-to-roll printing of polymer TFTs on kaolin-coated packaging paper.[2] The majority of the organic TFTs fabricated on paper in the past have required operating voltages of at least 10 V,[13,16,20] which is likely too high for most of the applications envisioned for paper electronics, as these are primarily targeting mobile or wearable devices powered by small batteries or energy-harvesting concepts. One possibility to reduce the operating voltage of organic TFTs and circuits is the use of electrolyte-gated or electrochemical TFTs,[7,10,21] while electrolyte-gated and electrochemical TFTs can provide very large transconductances at very low operating voltages,[22] they usually suffer from large signal delays, as they involve the inherently slow movement of ions. Another option for fabricating low-voltage organic TFTs and circuits is to utilize very thin gate dielectrics,[23] e.g., consisting of a thin aluminum oxide layer and a self-assembled monolayer of alkylphosphonic acids, and following this approach, organic transistors and inverters have previously been demonstrated on paper.[6,24]

Here, we report on the current–voltage characteristics and the contact resistance of low-voltage p- and n-channel organic

Dr. U. Kraft, Dr. H. Klauk
Max Planck Institute for Solid State Research
70569 Stuttgart, Germany
E-mail: ukraft@stanford.edu
Dr. U. Kraft, Prof. E. Weber
Institute for Organic Chemistry
Technical University Freiberg
09596 Freiberg, Germany
Dr. U. Kraft, Prof. B. Murmann
Department of Electrical Engineering
Stanford University
Stanford, CA 94305, USA
Dr. T. Zaki, Dr. F. Letzkus, Prof. J. N. Burghartz
Institut für Mikroelektronik Stuttgart (IMS CHIPS)
70569 Stuttgart, Germany

**ADVANCED
SCIENCE NEWS**

www.advancedsciencenews.com

**ADVANCED
ELECTRONIC
MATERIALS**

www.advelectronicmat.de

TFTs and on the dynamic performance of low-voltage unipolar and complementary organic ring oscillators fabricated on banknotes. The TFTs were fabricated in the bottom-gate, top-contact architecture. The gate dielectric consists of a plasma-grown aluminum oxide layer and a self-assembled monolayer (SAM) of an alkyl- or fluoroalkylphosphonic acid and has a thickness of 5.4 nm (in the case of an alkylphosphonic acid) or 5.7 nm (fluoroalkylphosphonic acid). A small gate-dielectric thickness is beneficial in terms of the low-voltage operation and the mechanical bendability of the TFTs. Organic p-channel and n-channel TFTs were fabricated using the vacuum-deposited small-molecule semiconductors dinaphtho[2,3-b:2′,3′-f] thieno[3,2-b]thiophene (DNTT)[25–29] and N,N'-bis(2,2,3,3,4,4,4) heptafluorobutyl-1,7-dicyano-perylene-(3,4:9,10)-tetracarboxylic diimide (Polyera ActivInk N1100),[25,30,31] respectively. These semiconductors were chosen for their relatively high carrier mobilities and good shelf-life stability.[32,33] The TFTs and ring oscillators were fabricated by stencil lithography.[25,27]

2. Results and Discussion

2.1. Static Characteristics of p-Channel DNTT TFTs on Banknotes

Figure 1 shows the output and transfer characteristics of a DNTT TFT fabricated using an alkylphosphonic acid

gate-dielectric SAM on a 5-Euro banknote. The channel length (L) and width (W) are 100 µm and the gate-to-contact overlap (L_C) is 20 µm. The TFT has an effective carrier mobility of 1.1 cm^2 (Vs)$^{-1}$, a threshold voltage of −1.4 V, an on/off current ratio of 10^5, and a subthreshold swing of 103 mV (dec)$^{-1}$. The gate current is below 1 nA, confirming the good quality of the hybrid oxide/SAM gate dielectric. The output characteristics show that the drain current increases linearly for small drain-source voltages and saturates at larger drain-source voltages. Results of a bias-stress measurement are shown in Figure S1 in the Supporting Information.

To investigate the stability of the transistors against mechanical bending of the substrate, the transfer characteristics of a DNTT TFT were measured before, during and after outward bending. The TFT has a channel length of 100 µm and a channel width of 100 µm. For the bending experiment, the banknote was rolled around a cylindrical bar with a radius of about 2.5 mm, which induces a tensile strain of about 3% in the TFTs. The effect of the bending on the transfer characteristics can be seen in Figure 1: The carrier mobility and the drain current measured at a gate-source voltage of −3 V are 1.12 cm^2 (Vs)$^{-1}$ and 0.95 µA prior to bending, 0.91 cm^2 (Vs)$^{-1}$ and 0.76 µA in the bent state, and 1.08 cm^2 (Vs)$^{-1}$ and 0.9 µA in the flat state after bending. There appears to be no systematic effect of the bending on the threshold voltage and the gate current. A summary of the device parameters before, during and after bending
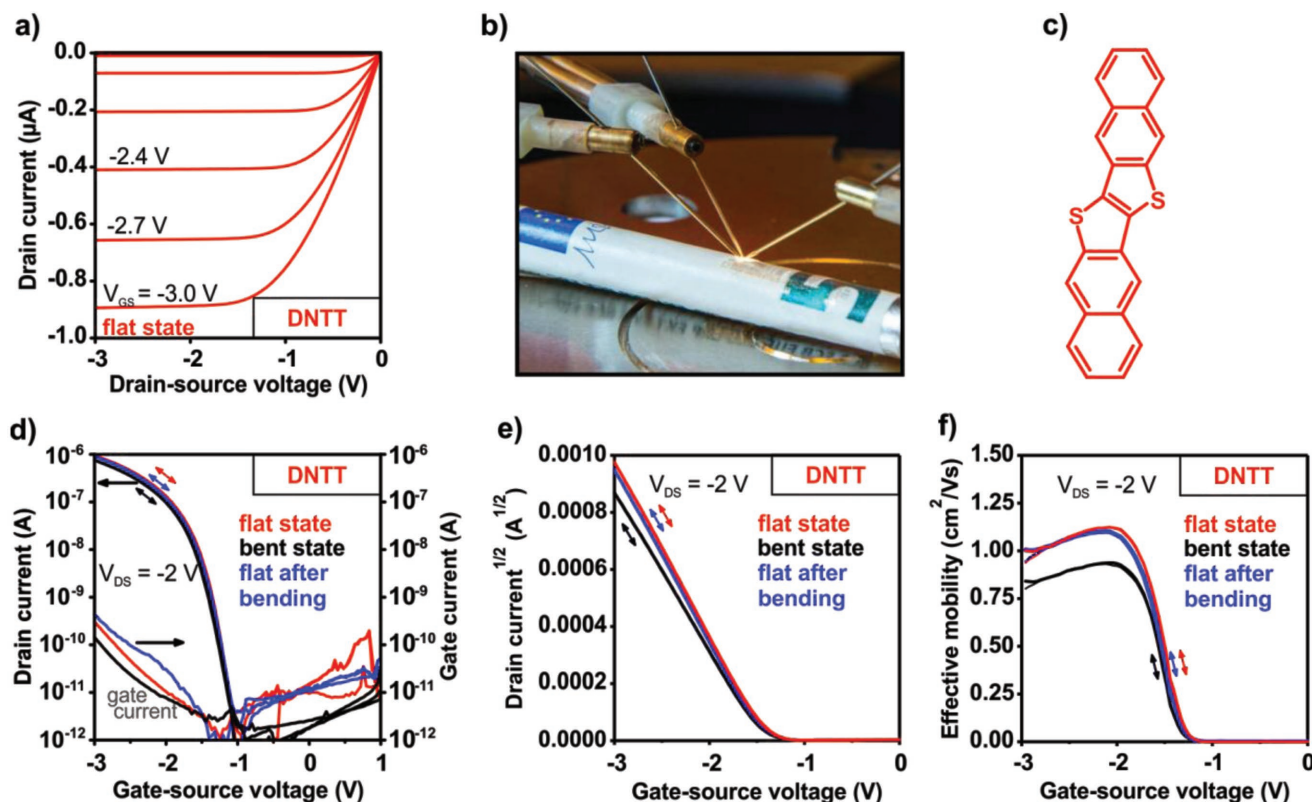

Figure 1. Output and transfer characteristics of a p-channel DNTT TFT with a channel length of 100 µm and a channel width of 100 µm fabricated on a banknote. a) Output characteristics measured before bending. b) Photograph of the measurement in the bent state. c) Molecular structure of the organic semiconductor DNTT. d,e) Transfer characteristics recorded before, during and after bending. f) Differential carrier mobility plotted as a function of gate-source voltage.
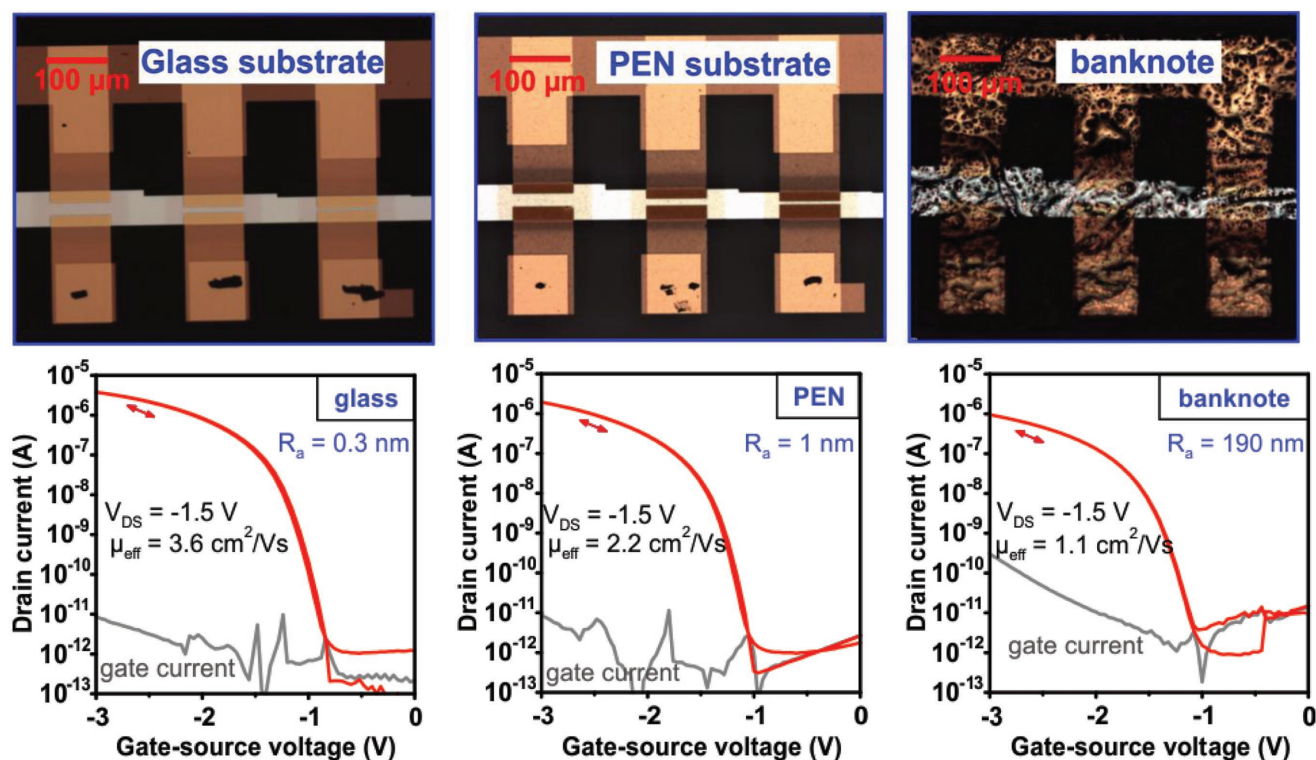
Figure 2. Photographs and transfer characteristics of p-channel DNTT TFTs fabricated on glass, PEN, and a banknote. The TFTs have a channel length of 100 µm and a channel width of 100 µm.

is given in Table S1 in the Supporting Information. The relative degradation of the carrier mobility and the drain current upon bending is similar to what has been reported in the literature for organic TFTs for similar bending strains.[34–37]

The relation between the channel length of the DNTT TFTs (ranging from 1 to 100 µm) and the effective carrier mobility (μ_{eff}) is shown in Figure S2 in the Supporting Information. As can be seen, the effective mobilities range from 1.1 cm² (Vs)$^{-1}$ ($L = 100$ µm) to 0.58 cm² (Vs)$^{-1}$ ($L = 10$ µm) and 0.13 cm² (Vs)$^{-1}$ ($L = 1$ µm). This dependence of the effective mobility on the channel length originates from the relative influence of the contact resistance: A smaller channel length results in a smaller channel resistance, but since the contact resistance is independent of the channel length, the effective carrier mobility decreases with decreasing channel length.[38–41] Using the transmission line method (TLM),[25,27,39–43] we have determined a width-normalized contact resistance of 1.4 kΩ cm and an intrinsic channel mobility of 0.8 cm² (Vs)$^{-1}$ at an overdrive voltage ($V_{GS}−V_{th}$) of −1.3 V for the DNTT TFTs (see also Table S2 in the Supporting Information).

To examine how the electrical characteristics of organic TFTs are affected by the surface roughness of the substrate,[44–47] we fabricated DNTT TFTs using the same materials and the same fabrication process on three different substrates characterized by significantly different surface roughness: glass (RMS roughness 0.3 nm), polyethylene naphthalate (PEN; RMS roughness 1 nm), and a banknote (RMS roughness 190 nm). The surface roughness of each substrate was determined from a line measurement performed using a profilometer over a lateral distance of 40 µm.

The obtained root mean square (RMS) and arithmetical mean (R_a) values of the surface roughness are listed in Table S3 in the Supporting Information.

Figure 2 shows the measured transfer characteristics of DNTT TFTs fabricated on the three different substrates. The effective carrier mobilities, threshold voltages, and subthreshold swings are summarized in **Table 1**. The highest effective mobility was obtained on the glass substrate (3.6 cm² (Vs)$^{-1}$), followed by the PEN substrate (2.2 cm² (Vs)$^{-1}$) and the banknote (1.1 cm² (Vs)$^{-1}$). The effect of the surface roughness on the carrier mobility is thus clearly observed (see also Figure S3 in the Supporting Information); it can be attributed to the detrimental effect of the surface roughness on the degree of molecular ordering in the organic semiconductor film.[41] Similarly, the surface roughness of the substrate also affects the gate current of the TFTs: At a gate-source voltage of −3 V, the gate current is about 10 pA for the TFTs on the glass and PEN substrates, but 300 pA for the TFTs on the banknote. The magnitude of the gate current is likely related to the density of structural defects in the gate dielectric induced by the surface topology of the substrate.

In TFTs fabricated in the staggered device architecture, the contact resistance generally depends on the intrinsic channel mobility, which can be explained in the framework of the current-crowding model.[48–51] To examine this relation, we used the TLM to determine the contact resistance and the intrinsic channel mobility of the DNTT TFTs fabricated on glass, PEN, and a banknote. The results are included in Table 1. As expected, the TFTs on glass have the largest intrinsic channel mobility (3.9 cm² (Vs)$^{-1}$) and the smallest contact resistance

**ADVANCED
SCIENCE NEWS**
www.advancedsciencenews.com

**ADVANCED
ELECTRONIC
MATERIALS**
www.advelectronicmat.de

Table 1. Electrical parameters of DNTT TFTs fabricated on glass, PEN, and a banknote.

Substrate	Glass	PEN	Banknote
Surface roughness			
R_q	0.34 nm	1 nm	189 nm
R_a	0.27 nm	0.8 nm	146 nm
Electrical characteristics of TFTs with $L = 100\,\mu m$, $W = 100\,\mu m$, $L_C = 20\,\mu m$			
Saturation region ($V_{DS} = -1.5$ V)			
Max. effective mobility	3.6 cm^2 (Vs)$^{-1}$	2.2 cm^2 (Vs)$^{-1}$	1.1 cm^2 (Vs)$^{-1}$
Threshold voltage	−1.2 V	−1.4 V	−1.4 V
Subthreshold swing	92 mV (dec)$^{-1}$	85 mV (dec)$^{-1}$	103 mV (dec)$^{-1}$
Linear region ($V_{DS} = -0.1$ V)			
Max. effective mobility	2.99 cm^2 (Vs)$^{-1}$	2.1 cm^2 (Vs)$^{-1}$	1.06 cm^2 (Vs)$^{-1}$
Threshold voltage	−1.4 V	−1.2 V	−1.4 V
Subthreshold swing	99 mV (dec)$^{-1}$	100 mV (dec)$^{-1}$	115 mV (dec)$^{-1}$
TLM ($V_{DS} = -0.1$ V, $V_{GS} - V_{th} = -1.3$ V)			
Overdrive voltage ($V_{GS} - V_{th}$)	−1.3 V	−1.3 V	−1.3 V
Intrinsic mobility (μ_0)	3.9 ± 0.10 cm^2 (Vs)$^{-1}$	2.7 ± 0.15 cm^2 (Vs)$^{-1}$	0.8 ± 0.03 cm^2 (Vs)$^{-1}$
Width-normalized contact resistance ($R_C{*}W$)	0.43 ± 0.04 kΩ cm	0.91 ± 0.13 kΩ cm	1.4 ± 0.22 kΩ cm
Sheet resistance (R_{sheet})	278 ± 7 kΩ sq^{-1}	439 ± 24 kΩ sq^{-1}	1359 ± 45 kΩ sq^{-1}
Transfer length (L_T)	7.8 ± 0.7 μm	10.3 ± 0.1 μm	5.3 ± 0.8 μm
Coefficient of determination of the linear fit (R^2)	0.998	0.994	0.997

(0.43 kΩ cm), and the TFTs on the banknote have the smallest intrinsic channel mobility (0.9 cm^2 (Vs)$^{-1}$) and the largest contact resistance (1.4 kΩ cm).

2.2. Static Characteristics of n-Channel N1100 TFTs on Banknotes

Compared to unipolar circuits, complementary circuits provide significant advantages in terms of power consumption and noise margin.[52,53] Therefore, we also fabricated and investigated n-channel TFTs on banknotes, using Polyera ActivInk N1100 as the semiconductor.

As discussed previously,[25] N1100 TFTs have higher carrier mobilities when the gate dielectric is prepared using a fluoro-alkyl- rather than an alkylphosphonic acid SAM. A possible explanation is that the interactions between the fluoroalkyl substituents of the SAM and those of the semiconductor lead to a more favorable packing of the semiconductor.[54,55] As a result, complementary ring oscillators fabricated on PEN substrates using DNTT p-channel and N1100 n-channel TFTs showed shorter signal delays per stage when a fluoroalkyl rather than an alkyl SAM was employed for the gate dielectric.[25]

For this reason, all n-channel TFTs discussed here and all the TFTs in the complementary ring oscillators discussed below were fabricated using a fluoroalkyl SAM as part of the gate dielectric. The transfer and output characteristics of p-channel DNTT TFTs with a fluoroalkyl SAM are shown in Figure S4 (Supporting Information), and their electrical parameters

are included in Table S2 in the Supporting Information. The threshold voltages of the TFTs with the fluoroalkyl SAM are found to be more positive than those of the TFTs with the alkyl SAM, consistent with previous reports.[25,56–61]

Figure 3 shows the transfer and output characteristics of n-channel N1100 TFTs with two different channel lengths, 100 and 5 μm. The TFT with a channel length of 100 μm has an on/off current ratio of 4×10^5, a subthreshold swing of 173 mV (dec)$^{-1}$, and an effective carrier mobility of 0.17 cm^2 (Vs)$^{-1}$, which is to our knowledge the highest mobility reported to date for organic n-channel TFTs fabricated on paper. For a channel length of 5 μm, the effective mobility is smaller (0.05 cm^2 (Vs)$^{-1}$) and the output characteristics show an undesirable nonlinearity at small drain-source voltages, due to the greater influence of the contact resistance. Using TLM, a contact resistance of 41 kΩ cm and an intrinsic channel mobility of 0.24 cm^2 (Vs)$^{-1}$ were determined. However, even for this small channel length, the off-state drain current is very small (<1 pA) and the output characteristics show good saturation of the drain current at large drain-source voltages. Further results of the TLM characterization and a comparison to N1100 TFTs fabricated on PEN are summarized in Tables S2 and S4 in the Supporting Information.

2.3. Unipolar and Complementary Ring Oscillators on Banknotes

To evaluate the switching delays of the organic TFTs on paper, we fabricated and characterized 11-stage unipolar
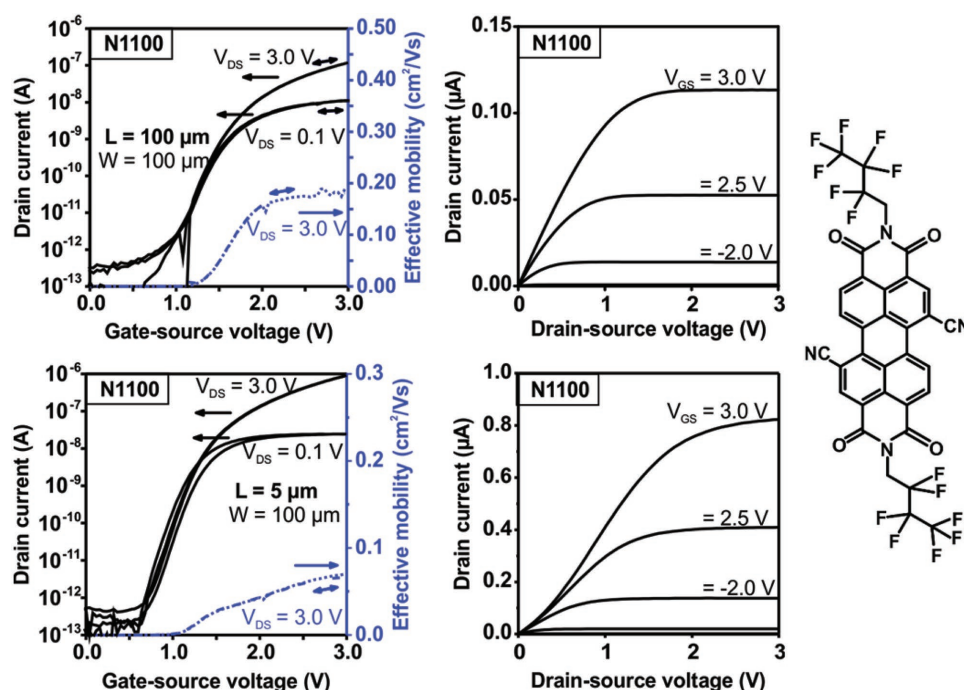
Figure 3. Transfer and output characteristics of n-channel N1100 TFTs with channel lengths of 100 and 5 µm fabricated on a banknote, and molecular structure of the organic semiconductor N1100.
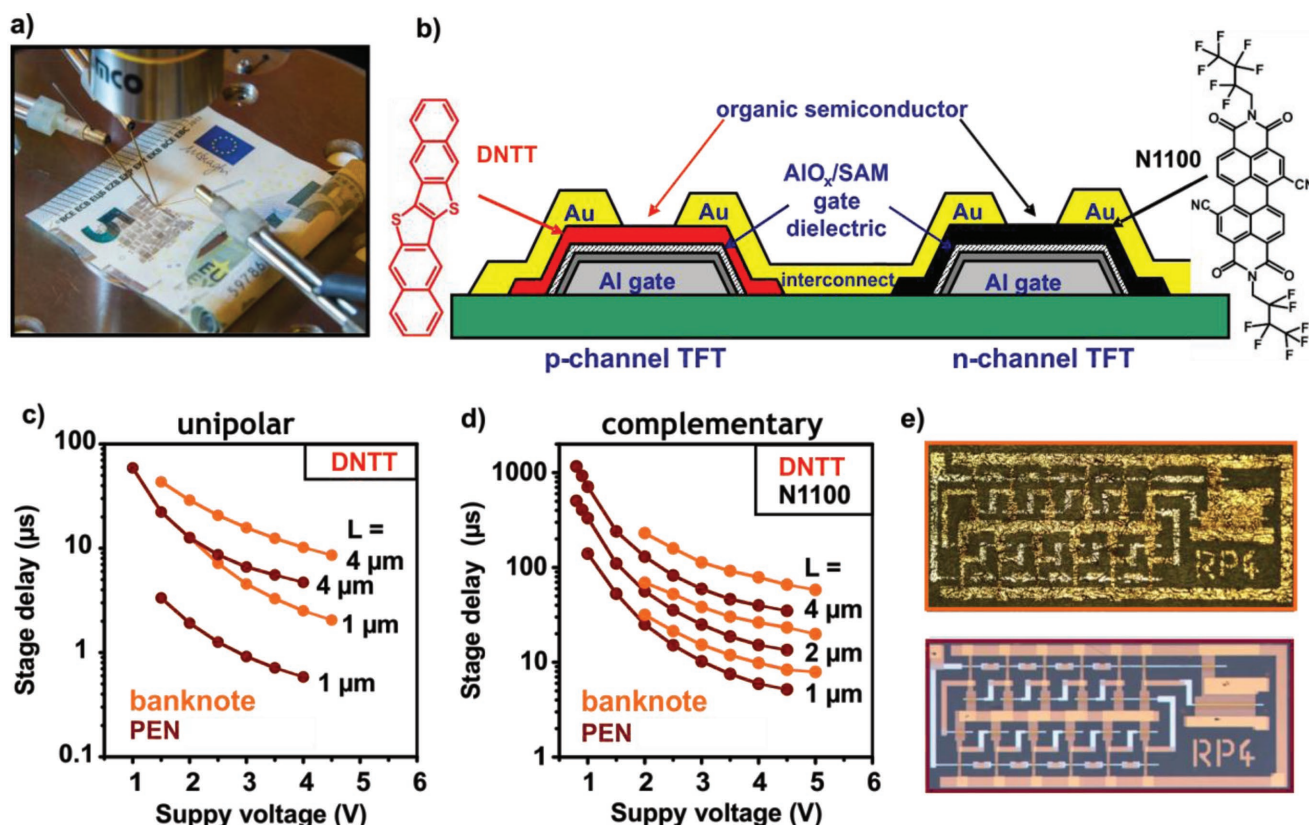

Figure 4. a) Photograph of a banknote with organic TFTs and circuits. b) Molecular structures of the organic semiconductors DNTT and Polyera ActivInk N1100, and schematic cross-section of the TFTs. c) Signal delay per stage measured in 11-stage unipolar ring oscillators fabricated on a banknote and on a PEN substrate. d) Signal delay per stage measured in 11-stage complementary ring oscillators fabricated on a banknote and on PEN. e) Photographs of unipolar ring oscillators fabricated on a banknote (top) and on PEN (bottom). The circuit has an area of approximately 5 mm × 2 mm.

1800453 (5 of 8)

ring oscillators based on p-channel DNTT TFTs and 11-stage complementary ring oscillators based on n-channel N1100 and p-channel DNTT TFTs with channel lengths of 4, 2, and 1 µm. The ring oscillators were fabricated on banknotes and, for comparison, on PEN substrates. The results are summarized in **Figure 4** and in **Table 2**.

Since the surface roughness of the substrate affects the carrier mobility of the TFTs (see Table 1), it also affects the signal delay of the ring oscillators. For example, for a channel length of 1 µm and a supply voltage of 4 V, the unipolar ring oscillators have stage delays of 2.5 µs on paper, compared to 580 ns on PEN, and the complementary ring oscillators have delays of 10 µs on paper, compared to 6 µs on PEN.[25] However, compared to earlier reports on organic circuits fabricated on paper

Table 2. Measured signal propagation delays per stage of unipolar and complementary ring oscillators fabricated on a banknote and on PEN substrates.

Channel length	Signal delay per stage at a supply voltage of 4 V			
	Unipolar ring oscillators		Complementary ring oscillators	
	Banknote	PEN	Banknote	PEN
$L = 4$ µm	10 µs	4.7 µs	79 µs	40 µs
$L = 2$ µm	n/a	n/a	26 µs	15 µs
$L = 1$ µm	2.5 µs	0.58 µs	10 µs	6 µs

(see **Table 3**), these ring oscillators operate with lower supply voltages and smaller signal delays.

Table 3. Literature overview of organic thin-film transistors on paper substrates.

	Type of paper	Semiconductor	Type	TFT geometry[a]	Operating voltage [V]	Carrier mobility [cm² (Vs)$^{-1}$]	On/off ratio	Subthreshold swing [V (dec)$^{-1}$]	Signal delay or cutoff frequency
[10]	coated photopaper	PEDOT:PSS	p	ECT	2	n/a	1×10^5	n/a	1 s (inverter)
[62]	paper	pentacene	p	BG/BC	30	0.2	10^6	1.8	12 ms (50 V; unipolar RO)
[11,12]	coated photopaper	P3HT	p	BG/BC	50	0.086	1×10^4	n/a	n/a
[7]	printer paper	PEDOT:PSS	p	ECT	2	n/a	10 µA	n/a	10 s (2 V; unipolar RO)
[19]	coated paper	P3HT	p	BC/TG	2	n/a	n/a	n/a	n/a
[6]	banknotes	DNTT	p	BG/TC	3	0.57	7×10^4	0.11	n/a
		$F_{16}CuPc$	n	BG/TC	3	0.005	1×10^4	n/a	n/a
[13]	coated photopaper	C_8-BTBT	p	BG/TC	40	1.3	1×10^8	2.0	n/a
[63]	PDMS coated banknotes	pentacene	p	BG/TC	15	0.12	5×10^3	n/a	n/a
[15]	homemade paper	NTCDI-$(CH_2C_7F_{15})_2$	n	BG/TC	100	0.0043	1×10^2	n/a	n/a
[18]	banknotes	pentacene	p	BG/TC	≥30	n/a	n/a	n/a	120 µs (50 V; compl. RO)
		PTCDI-$(C_8H_{17})_2$	n	BG/TC	≥30	n/a	n/a	n/a	
[16]	homemade paper	Merck Lisicon S1200	p	BG/BC	20	1.3	1×10^8	0.84	n/a
[2]	coated packaging paper	pBTTT	p	BG/BC	50	0.086	3×10^4	18.1	n/a
[20]	coated photopaper	C_8-BTBT	p	BC/TG	40	2.5	1×10^6	n/a	n/a
[7]	printer paper	DNTT	p	BG/TC	30	0.39	2×10^6	0.9	n/a
[9]	printer paper	DNTT	p	BG/TC	80	0.45	2×10^8	n/a	50 kHz (80 V,TFT)
[14]	photo paper, specialty paper	pentacene	p	BG/TC	55	0.09	1×10^5	n/a	n/a
[64]	CNC/glycerol + Al_2O_3	TIPS-pentacene: PTAA	p	BC/TG	10	0.23	3×10^3	n/a	n/a
[65]	glassine paper	P3HT	p	ECT	3	0.25	3×10^3	n/a	n/a
[22]	cleanroom paper	DNTT	P	BG/TC	2	1.6	1×10^6	0.090	n/a
[66]	PowerCoat HD 230 paper	TIPS-pentacene: PTAA	p	BC/TG	10	0.17	1×10^5	n/a	n/a
[17]	Starch paper	Pentacene, DNTT, PTAA	p	BC/TG	40	0.37	5×10^5	n/a	n/a
[67]	specialty paper	FS-0027	p	BC/TG	30	0.09	3×10^2	n/a	n/a
this work	Banknotes	DNTT	p	BG/TC	3	1.12	1×10^7	0.093	2.5 µs (4 V; unipolar RO)
		ActivInk N1100	n	BG/TC	3	0.17	4×10^6	0.17	10 µs (4 V; compl. RO)

[a]ECT = electrochemical transistor, BC = bottom-contact, TC = top-contact, BG = bottom-gate, TG = top-gate.

3. Conclusions

Organic p-channel and n-channel TFTs as well as unipolar and complementary ring oscillators were fabricated directly on the surface of a banknote. The use of a thin gate dielectric makes it possible to operate the TFTs with low voltages. Due to the rough surface of the banknotes, the charge-carrier mobilities are smaller than those of TFTs fabricated using the same semiconductors and gate dielectrics on smoother glass or PEN substrates, up to 1.1 cm^2 (Vs)$^{-1}$ for the p-channel TFTs and 0.17 cm^2 (Vs)$^{-1}$ for the n-channel TFTs. Bending tests have not revealed any significant changes in carrier mobility and gate current. For the first time, the contact resistance of organic TFTs on paper has been measured. At a supply voltage of 4 V, the unipolar and complementary ring oscillators operate with signal propagation delays as short as 2.5 and 10 μs per stage, respectively. These results show that it is possible to realize organic integrated circuits that can be operated with supply voltages of a few volts and frequencies of several hundred kilohertz directly on paper substrates.

4. Experimental Section

Materials: DNTT (dinaphtho[2,3-b:2′,3′-f]thieno[3,2-b]thiophene) and Polyera ActivInk N1100 [*N,N′*-bis(2,2,3,3,4,4,4)heptafluorobutyl-1,7-dicyano-perylene-(3,4:9,10)-tetracarboxylic diimide, PTCDI-(CN)$_2$-(CH$_2$C$_3$F$_7$)$_2$)] were purchased from Sigma Aldrich and Polyera, Skokie, IL, USA. *n*-Tetradecylphosphonic acid was purchased from PCI Synthesis, Newburyport MA, USA. 12,12,13,13,14,14,15,15,16,16,17,17,18,18,18-pentadecafluorooctadecylphosphonic acid was synthesized and kindly provided by Matthias Schlörholz., Corning Eagle 2000 glass substrates were purchased from Precision Glass & Optics, Santa Ana, CA, USA. 125 μm thick flexible polyethylene naphthalate foil (Teonex Q65 PEN) was kindly provided by William A. MacDonald, DuPont Teijin Films, Wilton, UK. 5-Euro banknotes were used as received.

Device Fabrication: Patterned aluminum gate electrodes with a thickness of 30 nm were deposited onto the substrates by thermal evaporation in vacuum. The thickness of the native aluminum oxide (AlO$_x$) layer was increased by a brief oxygen-plasma treatment (30 sccm O$_2$, 10 mTorr, 200 W, 30 s). The substrates were then immersed into a 2-propanol solution of either the alkyl or the fluoroalkylphosphonic acid molecules, which bind covalently to the AlO$_x$ surface and form a self-assembled monolayer (SAM). The resulting hybrid AlO$_x$/SAM gate dielectrics have a capacitance per unit area of 0.7 or 0.6 μF cm^{-2}, respectively.[25,42] Organic semiconductor films with a thickness of 20–25 nm were deposited onto these gate dielectrics by sublimation in vacuum with a rate of about 0.2 Å s^{-1}. During the deposition of the semiconductors, the substrate was held at a temperature of 60 °C for DNTT and 140 °C for N1100. The TFTs were completed by the vacuum deposition of gold source and drain contacts. All layers were patterned using silicon stencil masks.[25,27,68,69] The unipolar ring oscillators were fabricated using p-channel DNTT TFTs with a gate dielectric based on the alkylphosphonic acid SAM, while the complementary ring oscillators were fabricated using p-channel DNTT and n-channel N1100 TFTs with a gate dielectric based on the fluoroalkylphosphonic acid SAM.

Device Characterization: The surface roughness of the substrates was determined using a contact probe Dektak 150 profilometer over a lateral distance of 40 μm. The electrical measurements were performed in ambient air at room temperature under yellow laboratory light using a manual probe station and an Agilent 4156C Parameter Analyzer. The threshold voltages and effective carrier mobilities were calculated from the measured transfer curves by fitting drain-current equations for the linear and saturation regimes to the data. The contact resistances

and intrinsic carrier mobilities were determined using the transmission line method (TLM).

[1] D. Hunter, *Papermaking: The History and Technique of An Ancient Craft Courier Corporation*, Dover Publications, NY **1978**.

[2] G. Grau, R. Kitsomboonloha, S. L. Swisher, H. Kang, V. Subramanian, *Adv. Funct. Mater.* **2014**, *24*, 5067.

[3] Y. Lin, D. Gritsenko, Q. Liu, X. Lu, J. Xu, *ACS Appl. Mater. Interfaces* **2016**, *8*, 20501.

[4] Y. Zhang, P. Zuo, B. C. Ye, *Biosens. Bioelectron.* **2015**, *68*, 14.

[5] W. Dungchai, O. Chailapakul, C. S. Henry, *Anal. Chem.* **2009**, *81*, 5821.

[6] U. Zschieschang, T. Yamamoto, K. Takimiya, H. Kuwabara, M. Ikeda, T. Sekitani, T. Someya, H. Klauk, *Adv. Mater.* **2011**, *23*, 654.

[7] R. Mannerbro, M. Ranlöf, N. Robinson, R. Forchheimer, *Synth. Methods* **2008**, *158*, 556.

[8] B. Peng, P. K. Chan, *Org. Electron.* **2014**, *15*, 203.

[9] P. Peng, X. Ren, Z. Wang, X. Wang, R. C. Roberts, P. K. Chan, *Sci. Rep.* **2015**, *4*, 6430.

[10] P. Andersson, D. Nilsson, P. O. Svensson, M. Chen, A. Malmström, T. Remonen, T. Kugler, M. Berggren, *Adv. Mater.* **2002**, *14*, 1460.

[11] Y.-H. Kim, D.-G. Moon, J.-I. Han, *IEEE Electron Device Lett.* **2004**, *25*, 702.

[12] Y. Kim, D. Moon, W. Kim, J. Han, *J. Soc. Inf. Disp.* **2005**, *13*, 829.

[13] Y. Li, C. Liu, Y. Xu, T. Minari, P. Darmawan, K. Tsukagoshi, *Org. Electron.* **2012**, *13*, 815.

[14] A. T. Zocco, H. You, J. A. Hagen, A. J. Steckl, *Nanotechnology* **2014**, *25*, 094005.

[15] J. Huang, H. Zhu, Y. Chen, C. Preston, K. Rohrbach, J. Cumings, L. Hu, *ACS Nano* **2013**, *7*, 2106.

[16] Y. Fujisaki, H. Koga, Y. Nakajima, M. Nakata, H. Tsuji, T. Yamamoto, T. Kurita, M. Nogi, N. Shimidzu, *Adv. Funct. Mater.* **2014**, *24*, 1657.

[17] H. Jeong, S. Baek, S. Han, H. Jang, S. H. Kim, H. Sung Lee, *Adv. Funct. Mater.* **2018**, *28*, 1704433.

[18] L. Zhang, H. Wang, Y. Zhao, Y. Guo, W. Hu, G. Yu, Y. Liu, *Adv. Mater.* **2013**, *25*, 5455.

[19] R. Bollström, A. Määttänen, D. Tobjörk, P. Ihalainen, N. Kaihovirta, R. Österbacka, J. Peltonen, M. Toivakka, *Org. Electron.* **2009**, *10*, 1020.

[20] T. Minari, Y. Kanehara, C. Liu, K. Sakamoto, T. Yasuda, A. Yaguchi, S. Tsukada, K. Kashizaki, M. Kanehara, *Adv. Funct. Mater.* **2014**, *24*, 4886.

[21] J. Rivnay, S. Inal, A. Salleo, R. M. Owens, M. Berggren, G. G. Malliaras, *Nat. Rev. Mater.* **2018**, *3*, 17086.

[22] D. Khodagholy, J. Rivnay, M. Sessolo, M. Gurfinkel, M. P. Leleux, L. H. Jimison, E. Stavrinidou, T. Herve, S. Sanaur, R. M. Owens, G. G. Malliaras, *Nat. Commun.* **2013**, *4*, 2133.

[23] Y. M. Park, J. Daniel, M. Heeney, A. Salleo, *Adv. Mater.* **2011**, *23*, 971.

[24] U. Zschieschang, H. Klauk, *Org. Electron.* **2015**, *25*, 340.

[25] U. Kraft, M. Sejfić, M. J. Kang, K. Takimiya, T. Zaki, F. Letzkus, J. N. Burghartz, E. Weber, H. Klauk, *Adv. Mater.* **2015**, *27*, 207.

[26] Y. Yamamoto, K. Takimiya, *J. Am. Chem. Soc.* **2007**, *129*, 2224.

[27] F. Ante, D. Kälblein, T. Zaki, U. Zschieschang, K. Takimiya, M. Ikeda, T. Sekitani, T. Someya, J. N. Burghartz, K. Kern, *Small* **2012**, *8*, 73.

[28] U. Kraft, K. Takimiya, M. J. Kang, R. Rödel, F. Letzkus, J. N. Burghartz, E. Weber, H. Klauk, *Org. Electron.* **2016**, *35*, 33.

[29] W. Xie, K. Willa, Y. Wu, R. Häusermann, K. Takimiya, B. Batlogg, C. D. Frisbie, *Adv. Mater.* **2013**, *25*, 3478.

[30] B. A. Jones, M. J. Ahrens, M. H. Yoon, A. Facchetti, T. J. Marks, M. R. Wasielewski, *Angew. Chem., Int. Ed.* **2004**, *43*, 6363.

[31] J. Soeda, T. Uemura, Y. Mizuno, A. Nakao, Y. Nakazawa, A. Facchetti, J. Takeya, *Adv. Mater.* **2011**, *23*, 3681.

[32] U. Zschieschang, F. Ante, D. Kälblein, T. Yamamoto, K. Takimiya, H. Kuwabara, M. Ikeda, T. Sekitani, T. Someya, J. Blochwitz-Nimoth, H. Klauk, *Org. Electron.* **2011**, *12*, 1370.

[33] U. Zschieschang, K. Amsharov, M. Jansen, K. Kern, H. Klauk, R. T. Weitz, *Org. Electron.* **2015**, *26*, 340.

[34] K. Fukuda, Y. Takeda, M. Mizukami, D. Kumaki, S. Tokito, *Sci. Rep.* **2014**, *4*, 27450.

[35] T. Sekitani, Y. Kato, S. Iba, H. Shinaoka, T. Someya, T. Sakurai, S. Takagi, *Appl. Phys. Lett.* **2005**, *86*, 073511.

[36] T. Someya, T. Sekitani, S. Iba, Y. Kato, H. Kawaguchi, T. Sakurai, *Proc. Natl. Acad. Sci. USA* **2004**, *101*, 9966.

[37] A. N. Sokolov, Y. Cao, O. B. Johnson, Z. Bao, *Adv. Funct. Mater.* **2012**, *22*, 175.

[38] A. Fischer, H. Zündorf, F. Kaschura, J. Widmer, K. Leo, U. Kraft, H. Klauk, *Phys. Rev. Appl.* **2017**, *8*, 054012.

[39] D. Gundlach, L. Zhou, J. Nichols, T. Jackson, P. Necliudov, M. Shur, *J. Appl. Phys.* **2006**, *100*, 024509.

[40] T. Matsumoto, W. Ou-Yang, K. Miyake, T. Uemura, Takeya, *Org. Electron.* **2013**, *14*, 2590.

[41] R. Rödel, F. Letzkus, T. Zaki, J. N. Burghartz, U. Kraft, U. Zschieschang, K. Kern, H. Klauk, *Appl. Phys. Lett.* **2013**, *102*, 233303.

[42] U. Kraft, J. E. Anthony, E. Ripaud, M. A. Loth, E. Weber, H. Klauk, *Chem. Mater.* **2015**, *27*, 998.

[43] D. K. Schroder, *Semiconductor Material and Device Characterization*, Wiley, Hoboken, NJ **2008**.

[44] S. Steudel, S. De Vusser, S. De Jonge, D. Janssen, S. Verlaak, J. Genoe, P. Heremans, *Appl. Phys. Lett.* **2004**, *85*, 4400.

[45] C. Kim, A. Facchetti, T. J. Marks, *Science* **2007**, *318*, 76.

[46] K. Suemori, S. Uemura, M. Yoshida, S. Hoshino, N. Takada, T. Kodzasa, T. Kamata, *Appl. Phys. Lett.* **2008**, *93*, 033308.

[47] S. E. Fritz, T. W. Kelley, C. D. Frisbie, *J. Phys. Chem. B* **2005**, *109*, 10574.

[48] D. Natali, M. Caironi, *Adv. Mater.* **2012**, *24*, 1357.

[49] M. Marinkovic, D. Belaineh, V. Wagner, D. Knipp, *Adv. Mater.* **2012**, *24*, 4005.

[50] D. K. Schroder, *Semiconductor Material and Device Characterization*, John Wiley & Sons, Hoboken, NJ **2006**.

[51] T. J. Richards, H. Sirringhaus, *J. Appl. Phys.* **2007**, *102*, 094510.

[52] J. Zaumseil, H. Sirringhaus, *Chem. Rev.* **2007**, *107*, 1296.

[53] A. Petritz, A. Wolfberger, A. Fian, T. Griesser, M. Irimia-Vladu, B. Stadlober, *Adv. Mater.* **2015**, *27*, 7645.

[54] M. Sejfić, U. Kraft, N. H. Hansen, J. Pflaum, U. Zschieschang, H. Klauk, R. T. Weitz, *Electronic Materials Conference*, Santa Barbara, USA **2014**.

[55] J. W. Ward, R. Li, A. Obaid, M. M. Payne, D. M. Smilgies, J. E. Anthony, A. Amassian, O. D. Jurchescu, *Adv. Funct. Mater.* **2014**, *24*, 5052.

[56] U. Kraft, U. Zschieschang, F. Ante, D. Kälblein, C. Kamella, K. Amsharov, M. Jansen, K. Kern, E. Weber, H. Klauk, *J. Mater. Chem.* **2010**, *20*, 6416.

[57] K. Pernstich, S. Haas, D. Oberhoff, C. Goldmann, D. Gundlach, B. Batlogg, A. Rashid, G. Schitter, *J. Appl. Phys.* **2004**, *96*, 6431.

[58] S. Kobayashi, T. Nishikawa, T. Takenobu, S. Mori, T. Shimoda, T. Mitani, H. Shimotani, N. Yoshimoto, S. Ogawa, Y. Iwasa, *Nat. Mater.* **2004**, *3*, 317.

[59] M. Salinas, C. M. Jäger, A. Y. Amin, P. O. Dral, T. Meyer-Friedrichsen, A. Hirsch, T. Clark, M. Halik, *J. Am. Chem. Soc.* **2012**, *134*, 12648.

[60] S. K. Possanner, K. Zojer, P. Pacher, E. Zojer, F. Schürrer, *Adv. Funct. Mater.* **2009**, *19*, 958.

[61] C. Huang, H. E. Katz, J. E. West, *Langmuir* **2007**, *23*, 13223.

[62] E. Eder, H. Klauk, M. Halik, U. Zschieschang, G. Schmid, C. Dehm, *Appl. Phys. Lett.* **2004**, *84*, 2673.

[63] M. A. Khan, U. S. Bhansali, H. N. Alshareef, *Adv. Mater.* **2012**, *24*, 2165.

[64] C.-Y. Wang, C. Fuentes-Hernandez, J.-C. Liu, A. Dindar, S. Choi, J. P. Youngblood, R. J. Moon, B. Kippelen, *ACS Appl. Mater. Interfaces* **2015**, *7*, 4804.

[65] W. J. Hyun, E. B. Secor, G. A. Rojas, M. C. Hersam, L. F. Francis, C. D. Frisbie, *Adv. Mater.* **2015**, *27*, 7058.

[66] C.-Y. Wang, C. Fuentes-Hernandez, W.-F. Chou, B. Kippelen, *Org. Electron.* **2017**, *41*, 340.

[67] K. Y. Mitra, M. Polomoshnov, C. Martínez-Domingo, D. Mitra, E. Ramon, R. R. Baumann, *Adv. Electron. Mater.* **2017**, *3*, 1700275.

[68] F. Letzkus, J. Butschke, B. Höfflinger, M. Irmscher, C. Reuter, R. Springer, A. Ehrmann, J. Mathuni, *Microelectron. Eng.* **2000**, *53*, 609.

[69] T. Zaki, F. Ante, U. Zschieschang, J. Butschke, F. Letzkus, H. Richter, K. Klauk, J. N. Burghartz, *IEEE J. Solid-State Circuits* **2012**, *47*, 292.

1800453 (8 of 8)

Supporting Information

Low-Voltage, High-Frequency Organic Transistors and Unipolar and Complementary Ring Oscillators on Paper

Ulrike Kraft, Tarek Zaki, Florian Letzkus, Joachim N. Burghartz, Edwin Weber, Boris Murmann, Hagen Klauk
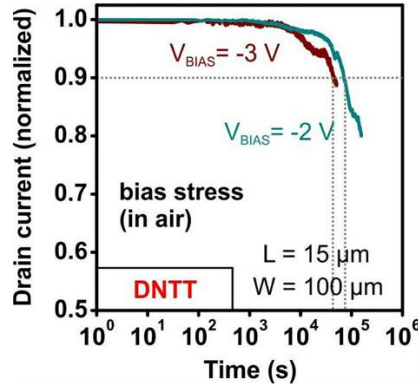
Table of Contents

1. Bias-Stress Stability of the TFTs

Figure S1. Bias stress stability of DNTT TFTs fabricated on a banknote ($V_{BIAS} = V_{GS} = V_{DS}$). The drain current decays faster when the applied gate-source voltage is larger, because larger gate-source voltages result in larger carrier densities in the channel and thus larger trapping rates.[32] (For comparison: For DNTT TFTs on a smoother PEN substrate it took 10^4 s for the drain current to decay by 10% for V_{BIAS} = -3V, and 10^5 s for V_{BIAS} = -2V.[32])

2. Bending Stability of the TFTs

Table S1: Device parameters of a DNTT TFT (L = 100 µm, W = 100 µm) before, during and after bending:

	Effective carrier mobility	Threshold voltage	Subthreshold swing	Drain current at V_{GS} = -3 V	Gate current at V_{GS} = -3 V
Before bending	1.1 cm²/Vs	-1.42 V	102 mV/dec	0.95 µA	0.3 nA
Bend state	0.9 cm²/Vs	-1.45 V	126 mV/dec	0.76 µA	0.1 nA
After bending	1.08 cm²/Vs	-1.44 V	111 mV/dec	0.90 µA	0.4 nA

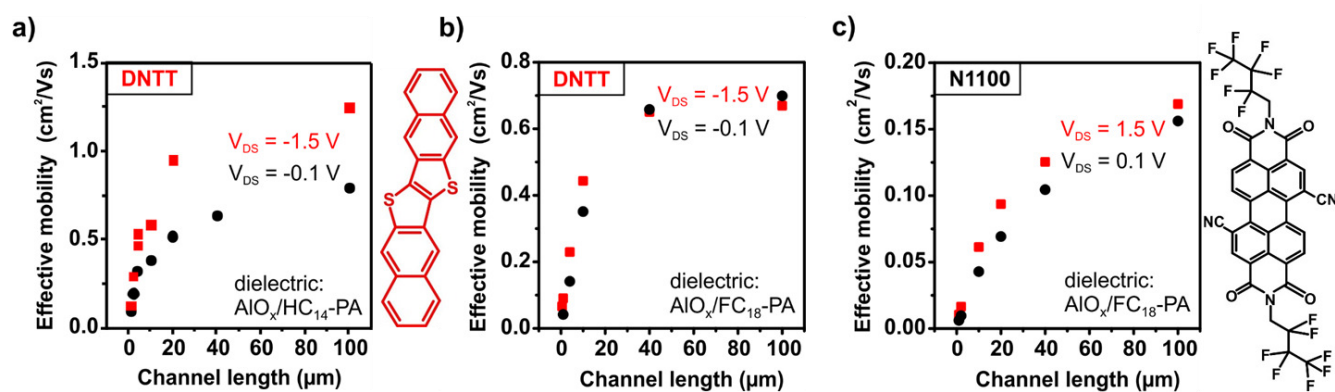## 3. Summary of the Characteristics of DNTT and N1100 TFTs on Banknotes

Figure S2. Effective mobility in dependence of the channel length for DNTT and N1100 TFTs at different drain-source voltages. a) DNTT p-channel TFTs with an alkylphosphonic acid SAM dielectric, b) DNTT p-channel TFTs with a fluoroalkylphosphonic acid SAM dielectric, c) N1100 n-channel TFTs with a fluoroalkylphosphonic acid SAM dielectric.

Table S2. Summary of the electrical characteristics of DNTT and N1100 TFTs on banknotes:

Semiconductor	DNTT		N1100
Dielectric	**alkyl SAM***	**fluoroalkyl SAM****	**fluoroalkyl SAM****
L = 100 µm, W = 100 µm, L_C = 20 µm, **V_{DS} = ±1.5 V)**			
V_{DS}	-1.5 V	-1.5 V	1.5 V
Max. effective mobility	1.13 cm^2/Vs	0.67 cm^2/Vs	0.17 cm^2/Vs
Threshold voltage	-1.4 V	0.2 V	1.4 V
Subthreshold swing	103 mV/dec	104 mV/dec	173 mV/dec
L = 100 µm, W = 100 µm, L_C = 20 µm, **V_{DS} = ±0.1 V**			
V_{DS}	-0.1 V	-0.1 V	0.1 V
Max. effective mobility	1.06 cm^2/Vs	0.70 cm^2/Vs	0.13 cm^2/Vs
Threshold voltage	-1.4 V	0.2 V	1.4 V
Subthreshold swing	115 mV/dec	108 mV/dec	180 mV/dec
[1]**Fit according to equation S1 (V_{DS} = ± 0.1 V)**			
[1]**Intrinsic mobility**	0.9 cm^2/Vs	0.81 cm^2/Vs	0.23 cm^2/Vs
[1]**$L_{1/2}$**	8.9 µm	12 µm	45 µm
[2]**TLM (V_{DS} = ± 0.1 V,)**			
Overdrive voltage (V_{GS}-V_{th})	-1.3 V	-1.3 V	1.3 V
[2]**Intrinsic mobility**	0.8 ± 0.03 cm^2/Vs	0.7 ± 0.04 cm^2/Vs	0.24 ± 0.02 cm^2/Vs
[2]**Width-normalized contact resistance**	1.4 ± 0.2 kΩcm	3.1 ±0.5 kΩcm	41 ± 2 kΩcm
[2]**Sheet resistance**	1400 + 100 kΩ/sq	1600 ± 100 kΩ/sq	5300 ± 400 kΩ/sq
[2]**Transfer length**	5 ± 1 µm	9 ± 2 µm	39 ± 4 µm
Coefficient of determination of the linear fit (R^2)	0.997	0.987	0.982

* alkylphosphonic acid SAM dielectric; ** fluoroalkylphosphonic acid SAM dielectric

4. Contact resistance

4.1 Effective Carrier and Intrinsic Channel Mobility

$L_{1/2}$ is the channel length at which the contact resistance equals the channel resistance, μ_{eff} is the effective mobility and μ_0 is the intrinsic mobility. The intrinsic mobility μ_0 can be determined by using the following equation:

$$\mu_{eff} = \frac{\mu_0}{1 + \dfrac{L_{1/2}}{L}} \qquad \text{(Equation S1)}$$

For further details, please refer to references 28, 37, 38 and 45.

4.2 Transmission Line Method

The intrinsic mobility, the width-normalized contact resistance, the sheet resistance and the transfer length have been determined by **TLM (transfer length or transmission line method)**. The contact resistance has been determined by performing resistance measurements on several TFTs in a ladder-type structure with different channel lengths and extrapolation of the resistance to a channel length of $L = 0$. The relationship between the channel resistance $R_{channel}$ and the sheet resistance R_{sheet} is described as follows:

$$R_{sheet} = \frac{R_{channel} \cdot W}{L} = \frac{1}{\mu_0 \cdot C_i \cdot (V_{GS} - V_{th})} \qquad \text{(Equation S2)}$$

where μ_0 is the intrinsic channel mobility (without the contribution of the contact resistance). For further details on the TLM, please refer to references 27, 28, 35-39, 44-46 and S1-S4.

5. Surface Roughness

Ra: Arithmetic mean height, average of the absolute profile height along the measured length

$$Ra = (1/L)\int_0^L Z(x)dx \qquad \text{(Equation S3)}$$

RMS, Rq: Root mean square average of the profile heights along the measured length

$$Rq = \sqrt{(1/L)\int_0^L Z(x)^2 dx} \qquad \text{(Equation S4)}$$

Compared with Ra, Rq is generally more strongly affected by a small number of large peaks and is thus generally larger than Ra.

Table S3: Surface roughness of the substrates utilized in this work:

Substrate:	Glass	PEN	Paper (banknote)
RMS (Rq):	0.34 nm	1 nm	189 nm
Ra:	0.27 nm	0.8 nm	146 nm

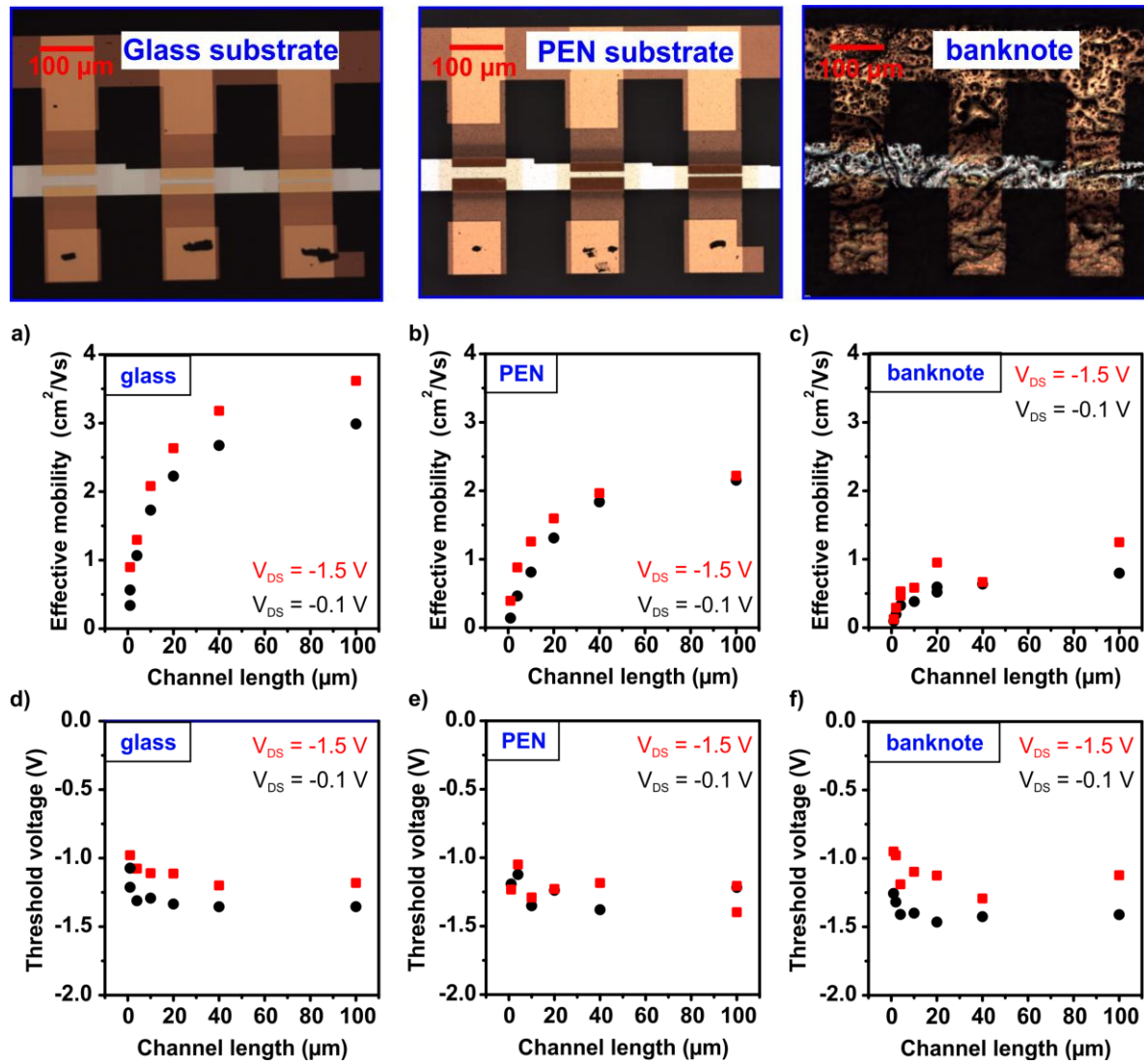## 6. Substrate-dependence of DNTT TFT parameters

Figure S3. Plot of a-c) the effective mobility and d-f) the threshold voltage versus the channel length of DNTT TFTs on glass, plastic (PEN) and paper (5 € banknote) substrates.

7. Substrate dependence of N1100 TFT parameters

Table S4. Electrical parameters of N1100 TFTs with a fluoroalkylphosphonic acid SAM dielectric fabricated on PEN and a banknote:

Substrate	PEN	Banknote
TFTs with L = 100 μm, W = 100 μm, L_C = 20 μm		
Saturation region (V_{DS} = 1.5 V)		
Effective mobility	0.26 cm^2/Vs	0.17 cm^2/Vs
Threshold voltage	0.9 V	1.4 V
Subthreshold swing	136 mV/dec	173 mV/dec
Linear region (V_{DS} = 0.1 V)		
Effective mobility	0.26 cm^2/Vs	0.13 cm^2/Vs
Threshold voltage	0.9 V	1.4 V
Subthreshold swing	147 mV/dec	180 mV/dec
Fits to TFTs with L = 1 μm to 100 μm, W = 100 μm, L_C = 20 μm		
Fit according to Equation S1 (V_{DS} = 0.1 V)		
Intrinsic mobility	0.38 cm^2/Vs	0.23 cm^2/Vs
$L_{1/2}$	47 μm	45 μm
TLM (V_{DS} = 0.1 V, V_{GS}-V_{th} = 1.3 V)		
Intrinsic mobility	0.4 cm^2/Vs	0.24 cm^2/Vs
Width-normalized contact resistance	31 kΩcm	41 kΩcm
Sheet resistance	3200 kΩ/sq	5300 kΩ/sq
Transfer length	49 μm	39 μm

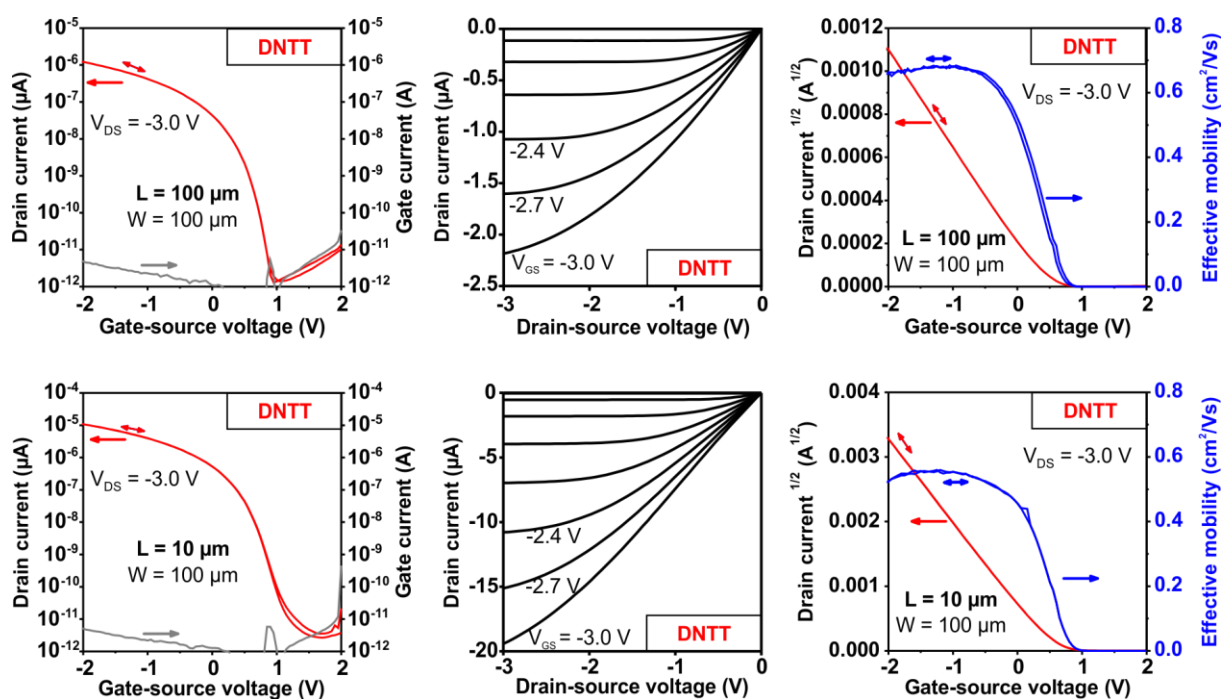## 8. DNTT TFTs with fluoroalkylphosphonic acid SAM dielectric

Figure S4. Transfer and output characteristics of p-channel DNTT TFTs with a fluoroalkyl-phosphonic acid SAM dielectric fabricated on a banknote. The TFTs have channel lengths of 100 µm (top row) and 10 µm (bottom row) and a channel width of 100 µm.

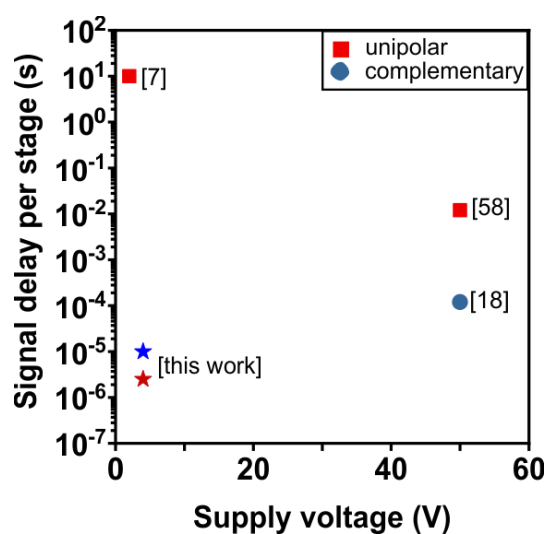## 9. Overview: Signal delay per stage of organic ring oscillators on paper

Figure S5. Signal delay per stage of organic ring oscillators fabricated on paper reported in the literature**.**

10. Additional References

[S1] Ante, F., Kälblein, D., Zschieschang, U., Canzler, T. W., Werner, A., Takimiya, K., Ikeda, M., Sekitani, Someya, T., Klauk, H. Contact Doping and Ultrathin Gate Dielectrics for Nanoscale Organic Thin-Film Transistors. Small **7**, 1186 (2011).

[S2] Berger, H. Contact resistance and contact resistivity. J. Electrochem. Soc. **119**, 507 (1972).

[S3] Chiang, C.-S., Martin, S. Kanicki, J., Ugai, Y., Yukawa, T., Takeuchi, S., Top-gate staggered amorphous silicon thin-film transistors: Series resistance and nitride thickness effects. Jpn. J. Appl. Phys. **37**, 5914 (1998).

[S4] Rödel, R., Letzkus, F., Zaki, T., Burghartz, J. N., Kraft, U., Zschieschang, U., Kern, K., Klauk, H. Contact properties of high-mobility, air-stable, low-voltage organic n-channel thin-film transistors based on a naphthalene tetracarboxylic diimide. Appl. Phys. Lett. **102**, 233303 (2013).